1993-03

Investigation of onset of plasma formation at anode of fast-pulsed high-voltage vacuum diode

Willis, Gregory

Monterey, California. Naval Postgraduate School

NAVAL POSTGRADUATE SCHOOL
Monterey, California

THESIS

Investigation of Onset of Plasma Formation
at Anode of Fast-Pulsed High-Voltage Vacuum Diode

by

Gregory Willis

March, 1993

Thesis Advisor: F. Schwirzke
Thesis Co-Advisor: X.K. Maruyama

Unclassified
SECURITY CLASSIFICATION OF THIS PAGE

REPORT DOCUMENTATION PAGE

1a. REPORT SECURITY CLASSIFICATION: Unclassified	1b. RESTRICTIVE MARKINGS
2a. SECURITY CLASSIFICATION AUTHORITY	3. DISTRIBUTION/AVAILABILITY OF REPORT: Approved for public release; distribution is unlimited.
2b. DECLASSIFICATION/DOWNGRADING SCHEDULE	
4. PERFORMING ORGANIZATION REPORT NUMBER(S)	5. MONITORING ORGANIZATION REPORT NUMBER(S)
6a. NAME OF PERFORMING ORGANIZATION: Naval Postgraduate School; 6b. OFFICE SYM: PH	7a. NAME OF MONITORING ORGANIZATION: Naval Postgraduate School
6c. ADDRESS (City, State, and ZIP Code): Monterey, CA 93943-5000	7b. ADDRESS (City, State, and ZIP Code): Monterey, CA 93943-5000
8a. NAME OF FUNDING/SPONSORING ORGANIZATION; 8b. OFFICE SYM (If applicable)	9. PROCUREMENT INSTRUMENT IDENTIFICATION NUMBER
8c. ADDRESS (City, State, and ZIP Code)	10. SOURCE OF FUNDING NUMBERS: PROGRAM ELEMENT NO.; PROJECT NO.; TASK NO.; WORK UNIT ACCESSION

11. TITLE (Include Security Classification)
INVESTIGATION OF ONSET OF PLASMA FORMATION AT ANODE OF FAST-PULSED HIGH-VOLTAGE VACUUM DIODE

12. PERSONAL AUTHOR(S)
GREGORY NMN WILLIS

13a. TYPE OF REPORT	13b. TIME COVERED	14. DATE OF REPORT (Year,Month,Day)	15. PAGE COUNT
Master's Thesis	FROM _____ TO _____	March 1993	62

16. SUPPLEMENTARY NOTATION
The views expressed in this thesis are those of the author and do not reflect the official policy or position of the Department of Defense or the U.S. Government.

17. COSATI CODES			18. SUBJECT TERMS (Continue on reverse if necessary and identify by block number)
FIELD	GROUP	SUB-GROUP	vacuum diode; anode spot; cathode spot; space charge; onset of

19. ABSTRACT (Continue on reverse if necessary and identify by block number)

The mechanism by which plasma forms in a fast pulsed high vacuum diode has been greatly studied. For the most part, efforts have been concentrated on plasma formation at the cathode. Recently, investigators improved the popular explosive emission model, taking into account the ion current density and surface heating through ion bombardment. This model provides total current densities of the order necessary for exploding whiskers on the cathode surface, and explains the cathode spot phenomena. The general belief is that a fast pulsed high voltage diode event is dominated by cathodic processes, and little research into plasma formation at the anode has been conducted. This study presents experimental results which support the above model applied to both the cathode and anode regions of the diode. It is shown here that plasma formation does indeed take place in the anode region, and, that the formation occurs nearly simultaneously with plasma formation at the cathode. Also, photographic evidence of post-breakdown cratering on the anode surface, similar to the cathode spot phenomena, will be presented.

20. DISTRIBUTION/AVAILABILITY OF ABSTRACT	21. ABSTRACT SECURITY CLASSIFICATION
[X] UNCLASSIFIED/UNLIMITED [ ] SAME AS RPT. [ ] DTIC USERS	Unclassified
22a. NAME OF RESPONSIBLE INDIVIDUAL: Fred Schwirzke	22b. TELEPHONE (Include Area Code): 408-656-2635; 22c. OFFICE SYMBOL: PH/Sw

DD Form 1473, JUN 86 — Previous editions are obsolete. S/N 0102-LF-014-6603 — SECURITY CLASSIFICATION OF THIS PAGE: Unclassified

Approved for public release; distribution is unlimited

INVESTIGATION OF ONSET OF PLASMA FORMATION AT ANODE OF FAST-PULSED HIGH-VOLTAGE VACUUM DIODE

by

Gregory Willis

Lieutenant , United States Navy
B.S., Tougaloo College, 1984

Submitted in partial fulfillment of the
requirements for the degree of

MASTER OF SCIENCE IN PHYSICS

from the

NAVAL POSTGRADUATE SCHOOL

March, 1993

Author: [redacted]
Gregory Willis

Approved by: [redacted]
Fred Schwirzke, Thesis Advisor

[redacted]
X. K. Maruyama, Thesis Co-Advisor

[redacted]
Karlheinz E. Woehler, Chairman,

ABSTRACT

The mechanism by which plasma forms in a fast pulsed high vacuum diode has been greatly studied. For the most part, efforts Recently, investigators improved the popular explosive emission model, taking into account the ion current density and surface heating through ion bombardment. This model provides total current densities of the order necessary for exploding whiskers on the cathode surface, and explains the cathode spot phenomena. The general belief is that a fast pulsed high voltage diode event is dominated by cathodic processes, and little research into plasma formation at the anode has been conducted. This study presents experimental results which support the above model applied to both the cathode and anode regions of the diode. It is shown here that plasma formation does indeed take place in the anode region, and, that the formation occurs nearly simultaneously with plasma formation at the cathode. Also, photographic evidence of post-breakdown cratering on the anode surface, similar to the cathode spot phenomena, will be presented.

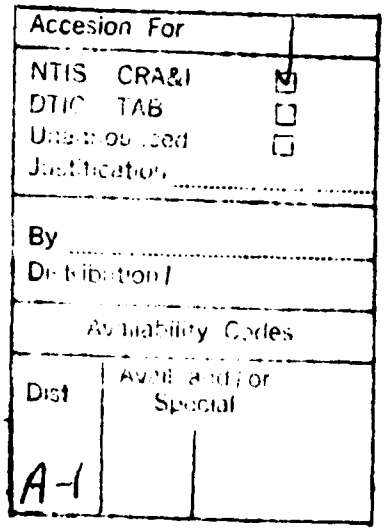

TABLE OF CONTENTS

ACKNOWLEDGMENTS

The completion of this thesis is due to the support and efforts of several people to whom I would like to express my deep appreciation. My thanks to Dr. Schwirzke, for his inspiration and theoretical guidance. And to Dr. Maruyama for his technical guidance and support, and for letting me use all of his 'stuff'. My thanks to Harold Rietdyk and Don Snyder for always being there for whatever I needed. And, to George Jaksha for his assistance with materials, but mostly for his ever-present and uplifting sense of humor. Lastly, and most certainly not in the least, my thanks to Eva and Mercedes for keeping me on top of all those little pink notes that I tried so hard to ignore. My best wishes to you all.

Greg Willis

24 March 1993

I. INTRODUCTION

The breakdown of and formation of plasmas on electrode surfaces is fundamental to pulsed power applications. High voltage, high current particle beam sources now operate in nanosecond time frames, between plasma formation and diode gap closure. Breakdown of the cathode surface in a fast-pulsed high voltage vacuum diode has been greatly studied in recent years. Post-breakdown cathode surface conditions can be explained by unipolar arcing [Ref. 1-3], however, the events leading to breakdown are not well understood. An understanding of pre-breakdown processes and the ability to predict the occurrence of breakdown and the onset of plasma formation is necessary for the precise design of diodes specific to a given application.

Previous work at the Naval Postgraduate School Flash X-Ray facility proposed a new model for Cathode Spot Formation [Ref. 2]. This model describes the pre-breakdown stages, and explains the presence of craters on the cathode surface subsequent to a high voltage pulse across the diode (unipolar arcing). It incorporates the effects of ion heating, providing a total current density sufficient to explode a whisker within a few nanoseconds.

It is generally believed that cathodic processes dominate fast pulsed diode events. This model does not address events occurring in the anode region of the diode.

The purpose of this study is to investigate the events taking place at the anode; specifically, to determine if plasma formation occurs at the anode, and if so, to determine the time of plasma formation. This data will then be compared to experimental data (obtained as part of this study) on plasma formation at the cathode, and, to the predictions of the cathode spot formation model.

II. REVIEW OF PLANAR DIODE PHYSICS

Planar diodes are composed of two parallel plates (electrodes) separated by a distance which is small relative to the electrodes' dimensions. In this review, several topics will be discussed in separate sections. These topics are those most relevant to both planar diode physics and the experiments in this work.

A. ELECTRIC FIELD

When there is no current through the diode, the electric field, E, is given by

$$E = \frac{\Phi_o}{d} \tag{2.1}$$

where Φ_o is the applied voltage across the diode, and d is the gap spacing. Once current is flowing through the diode, the electric field and potential are a function of the presence of positively and negatively charged particles (space charge) in the gap. One effect of this space charge is to limit the current density in the diode [Ref. 4]. The general effect results in a potential minimum near the cathode, which increases with time [Ref. 4].

B. SPACE CHARGE LIMITED CURRENT DENSITY

As mentioned previously, the buildup of space charge in the diode limits the maximum current density which can

flow between the electrodes. The Child-Langmuir equation [Ref. 4] deals with this phenomenon in a relativistic manner. For the experiments in this work the non-relativistic Child-Langmuir current density limit is given by

$$j_{cl} = \frac{4}{9}\varepsilon_0(2\frac{e}{m})^{\frac{1}{2}}\frac{\Phi o^{\frac{3}{2}}}{d^2}, \qquad (2.2)$$

where

ε_0≡permittivity of free space =8.85x10^{-12} F/m;

e≡magnitude of elementary charge;

m≡mass of the charge carrier;

Φ_0≡applied potential voltage; and

d≡diode gap

C. FIELD EMISSION

In the presence of a sufficiently strong electric field (E>10^7 V/m), electrons will be emitted from the cold cathode and accelerated towards the anode. This process is known as field emission and is quantified by the Fowler-Nordheim equation. The result which is pertinent here is the relationship between the magnitude of the electric field and the emitted current density. This relationship is given by

$$j_{fe} = c_1 \beta^2 E^2 \exp\left(-\frac{c_2}{\beta E}\right) \qquad (2.3)$$

where

j_{fe} ≡ field emitted current density;

β ≡ field enhancement factor;

c_1, c_2 ≡ numerical constants; and

E ≡ applied electric field.

Note that for large electric fields, the current density is essentially proportional to the square of the E-field [Ref. 4].

D. PARAPOTENTIAL FLOW

Parapotential flow describes the effect of azimuthal self magnetic fields produced from high current flow through the diode. In the case of electron charge carriers, a self focusing effect results. The presence of parapotential flow complicates the problem significantly. The maximum electron flow for which this effect may be ignored is given by

$$I_c = 2\pi\varepsilon_0 \frac{\gamma m c^3}{e} \frac{r_c}{d}, \qquad (2.4)$$

where

r_C≡cathode radius;

γ≡ Lorentz parameter;

c≡speed of light = 3×10^8 m/s;

d≡gap spacing;

e≡magnitude of charge

m≡mass of charge carrier [Ref. 4].

For this experiment the average voltage was 12 kA, which is less than the critical value of 18.5 kA. For the configuration of the NPS Flash X-Ray machine used in the experiments of this work, the self magnetic field is negligible and parapotential flow is ignored.

F. RELATIVITY

A diode is considered relativistic if a charged particle in the diode gap is accelerated to velocities near the speed of light. The electron, with its significantly smaller mass, will have the highest velocity of all the particles present in the gap, and its behavior would best characterize the diode.

The most common method to characterize the relativistic nature of a charged particle is through it's Lorentz parameter, γ, given by

$$\gamma = \frac{1}{\sqrt{1 - \frac{v^2}{c^2}}} \qquad (2.5)$$

where c is the speed of light in a vacuum and v is the particle's velocity. For a charged particle in an electric field, γ can be written as

$$\gamma = \gamma_o + \frac{e\Phi}{mc^2} \tag{2.6}$$

where

γ_o≡Lorentz parameter upon particle entering E-field;

Φ≡electric potential at specific position; and

e≡the magnitude of charge, and m is the particle's mass.

The particle can be said to behave relativistically for values of γ near 100, and nonrelativistically for values near 1. [Ref. 4]

III. MODEL FOR PLASMA FORMATION AND SURFACE INTERACTION

The model proposed by Hallal [Ref. 2] describes the early stages leading to plasma formation and plasma interaction with the cathode surface which results in the well studied cathode spot. Here, plasma formation at the anode will be considered, based on that model.

A. DIODE CONDITIONS

It must be noted that diode surfaces are far from high vacuum clean. Adsorbates are weakly bound to the surface, which, although polished, still has numerous microscopic irregularities. In the presence of a sufficiently high electric field, $E>10^7 V/m$, whiskers, dust particles, oxide spots and other nonuniformities present on the electrode surface provide enhanced field emission of electrons. This field emission, the electric field, and surface bombardment by ions stimulate desorption of neutrals. Due to the pressure differential, these neutrals then move away from the electrode surface and form a dense neutral gas moving with sound velocity $v \approx 330$ m/s. (See Figure 3.1) The neutral gas layer will then be ionized by the field emitted electrons when the ionization cross section becomes sufficient [Ref. 5]

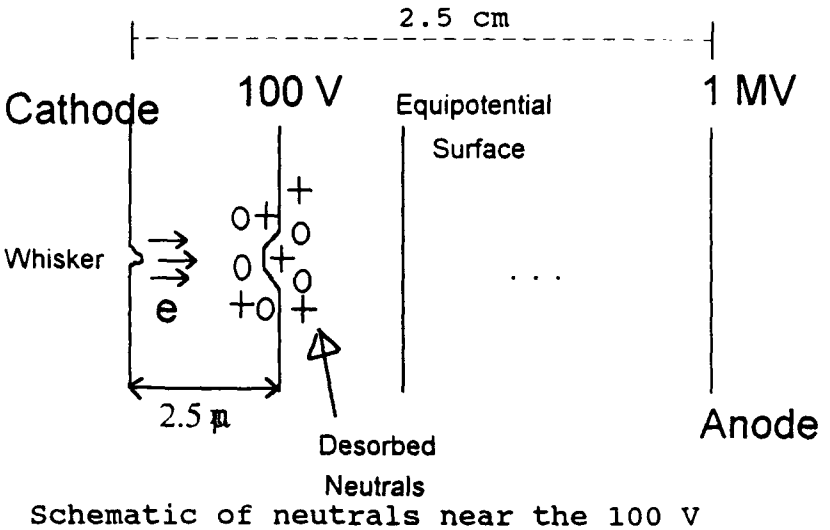

Figure 3.1 Schematic of neutrals near the 100 V equipotential surface. Here, the ionization cross section is at its maximum value [Refs. 2,4,5]

B. THE MODEL

The diode has a gap spacing of 2.5 cm across which a 1 MV potential is applied. The electric field produced by this potential is 40 MV/m or 0.40 MV/cm, and is assumed to be uniform and constant within the gap. The source for the field emitted electrons are the whiskers present on the cathode surface. The electrons, accelerating towards the anode, and the pressure differential in the diode chamber cause the desorption and drift of neutrals away from the cathode. [Ref. 6]

The ionization cross section is a maximum around the 100 V potential surface [Ref. 5], which corresponds to 2.5 μm from the cathode. Figure 3.2 shows what may be typical

ionization cross section and neutral density profiles in the area of the cathode. Note that the ionization cross section approaches a maximum value very near the cathode surface.

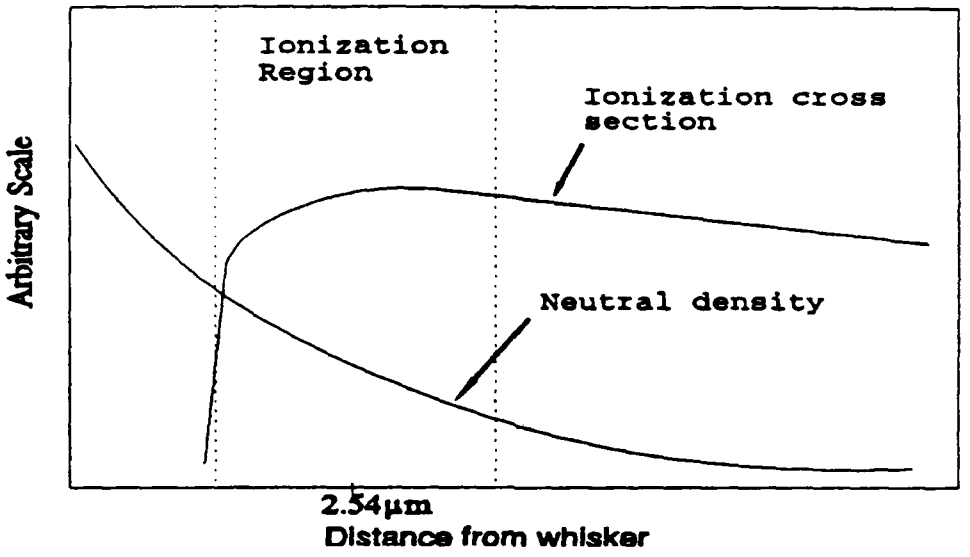

Figure 3.2 Ionization and Neutral Density curves as a function of distance from the cathode surface [Ref. 2]

The average position of ionization is the previously mentioned 2.5 μm distance from the cathode. The positively charged ions are then accelerated towards and bombard the cathode surface. Thereby heating the surface by means of ohmic heating and ion bombardment.

C. THE MODEL APPLIED TO THE ANODE

In extending the present model to the anode, similarities between the two cases must be noted. Firstly,

both anode and cathode surfaces will have similar characteristics, i.e. whiskers, impurities, etc.. Secondly, contaminates adsorbed on each surface will be similar prior to application of the potential. And, it is safe to assume that heating of the anode will occur initially by the displacement current, and once field emission sets in, by the arrival of energetic electrons. This coupled with the pressure differential in the diode will cause desorption of neutrals, and, as with events occurring at the cathode, the neutrals will form a dense gas moving away from the anode surface.

In the first few nanoseconds of the increasing voltage, the electrons at the cathode's surface see a potential less than the maximum of the voltage pulse, approximately 160 kV, at t=3 ns. These initial electrons are then accelerated towards the anode. These electrons also serve to further the desorption process and increase the local neutral density. Some of the fast electrons will ionize the neutral gas. Secondary electrons created a short distance away from the anode surface are accelerated towards the surface, gain energy and can then further ionize neutrals if the energy gain becomes greater than approximately 20-100 eV.

D. AFTER ONSET

After onset of plasma formation at each electrode, subsequent processes should develop in parallel as described by Hallal [Ref. 2]. The plasma formed through ionization of the dense neutral gas interacts with the electrode surfaces. The return bombardment of positive ions to the cathode and the bombardment of the anode by electrons leads to further desorption of neutrals, thereby further increasing the neutral densities. This will tend to increase the rate of ionization due to the decrease in mean free path length. The increase in initially slow ions present in front of the anode and cathode increases the positive space charge, enhancing the electric field near the cathode and, as described by the Fowler-Nordheim relation, enhances field emitted current. This process leads to the formation of a unipolar arc at the cathode. [Ref. 6] Plasma formation also occurs at the anode. The question is whether unipolar arcing can also occur at the anode-plasma interface? As mentioned previously, the anode surface will also be covered with adsorbates. Some of the energetic electrons arriving at the anode will desorb and ionize neutrals. Secondary electrons created by this ionization process and back scattered electrons (estimated at about 20% [Ref. 7]) further contribute to ionize particles at or very

near the anode surface. The heavy ions will be accelerated towards the cathode. Oxygen ions require approximately 10^{-8}s to reach the cathode if 1MV is applied over a gap of 2.5 cm. The ions created near the anode produce a positive space charge layer. This increases the potential in front of the anode. Field reversal is possible if the ionization rate becomes sufficiently high such that the electric field of the ion sheet becomes greater than the applied field. The electric field of the ion sheet is given by

$$E = \frac{1}{2}\varepsilon_0\sigma, \tag{3.1}$$

where σ is the charge density per unit area, i.e. C/m^2. A luminous plasma layer develops. Pressure gradients in the plasma and the condition of quasi-neutrality provide that the plasma assumes a positive potential with respect to the anode surface. This is exactly the same condition that exists for the plasma layer in front of the cathode. Unipolar arcs will be ignited. For a more detailed discussion of unipolar arc model, see Schwirzke in Reference 2.

E. MODEL PREDICTIONS

Reference 2 predicts a time delay for the onset of plasma formation at the cathode of 8 ns for a 1 MV pulse and 2.5 cm gap, as shown in Figure 3.3. The delay is measured from the onset of the voltage pulse to the onset of light

emission. This delay is based on the movement of the 100 V potential towards the cathode, and the expansion of the neutrals away from the cathode surface. The onset of plasma formation will occur when the 100 V equipotential surface and neutral gas reach the same location.

A similar kind of prediction for the formation of plasma at the anode is a more difficult matter. The rate of desorption is unknown. The effect of electron bombardment on that rate is also an unknown quantity. Therefore is it difficult at this juncture to predict when and where a sufficient neutral density will be reached for ionization. However, a couple of assumptions can be made which will serve to provide some boundary to the time of plasma onset at the anode.

For the applied electric field of 1 MV over the 2.5 cm gap (40 MV/m), the charge density required for the electric field of the ion sheet to cancel the applied field, is on the order of 4.4×10^{15} ions/m^2, by equation 3.1. The lifetime of oxygen ions, i.e. their time of flight is approximately 10^{-8} s. To have 4.4×10^{15} in the gap requires an ionization rate of 4.4×10^{23} ions/($m^2 \cdot s$).

Assuming that the electron current density is limited by the Child-Langmuir law to $j_{cl}=2.3 \times 10^{7}$ A/m^2 , the electron current density near the anode, approximately $j \leq enc$, corresponds to an electron flux of $nc=1.44 \times 10^{26}$ $e^-/(m^2 \cdot s)$. A

total number of 1.44×10^{28} (10^{-8} s) electrons must produce 4.4×10^{15} ions/($m^2 \cdot 10^{-8}$ s).

Therefore only about one ionization process per 330 impacting electrons is required to cancel the applied field in front of the anode. Higher ionization rates will result in field reversal.

One adsorbed monolayer has about 2.2×10^{19} neutral particles/m^2. Hence, the fraction of neutrals per monolayer and 10^{-8} s which must be ionized is $4.4 \times 10^{15}/2.2 \times 10^{19} = 2.2 \times 10^{-4}$. For 1 MeV electrons the ionization cross section is of the order $\sigma_o \approx 10^{-22}$ m^2. The particle density of adsorbed neutrals corresponds to $\eta_o \approx 10^{29}$ m^{-3}.

The ionization cross section and neutral densities given above correspond to a mean free path length of $\lambda \approx 1/(10^{29} \times 10^{-22}) = 10^{-7}$m or 0.1 μm. Since the width of one monolayer is $\approx 2.2 \times 10^{-10}$m, a fraction of $2.2 \times 10^{-10}/10^{-7} = 2.2 \times 10^{-3}$ neutrals has a chance to become ionized directly on the surface. For a number of $1.44 \times 10^{26}(10^{-8}) = 1.44 \times 10^{18}$ electrons arriving per m^2 per 10^{-8} s, a fraction of $1.44 \times 10^{18}(2.2 \times 10^{-3}/m^2) = 3.2 \times 10^{15}$ m^{-2} will produce ions. Hence the number of ions produced is of the same order as estimated (4.4×10^{15} ions/m^2 10^{-8}s) to start field reversal. This estimate of ionization rates neglected that several adsorbed monolayers probably exist on the anode surface. Furthermore, the ionization rate by backscattered and less energetic secondary electrons has been neglected.

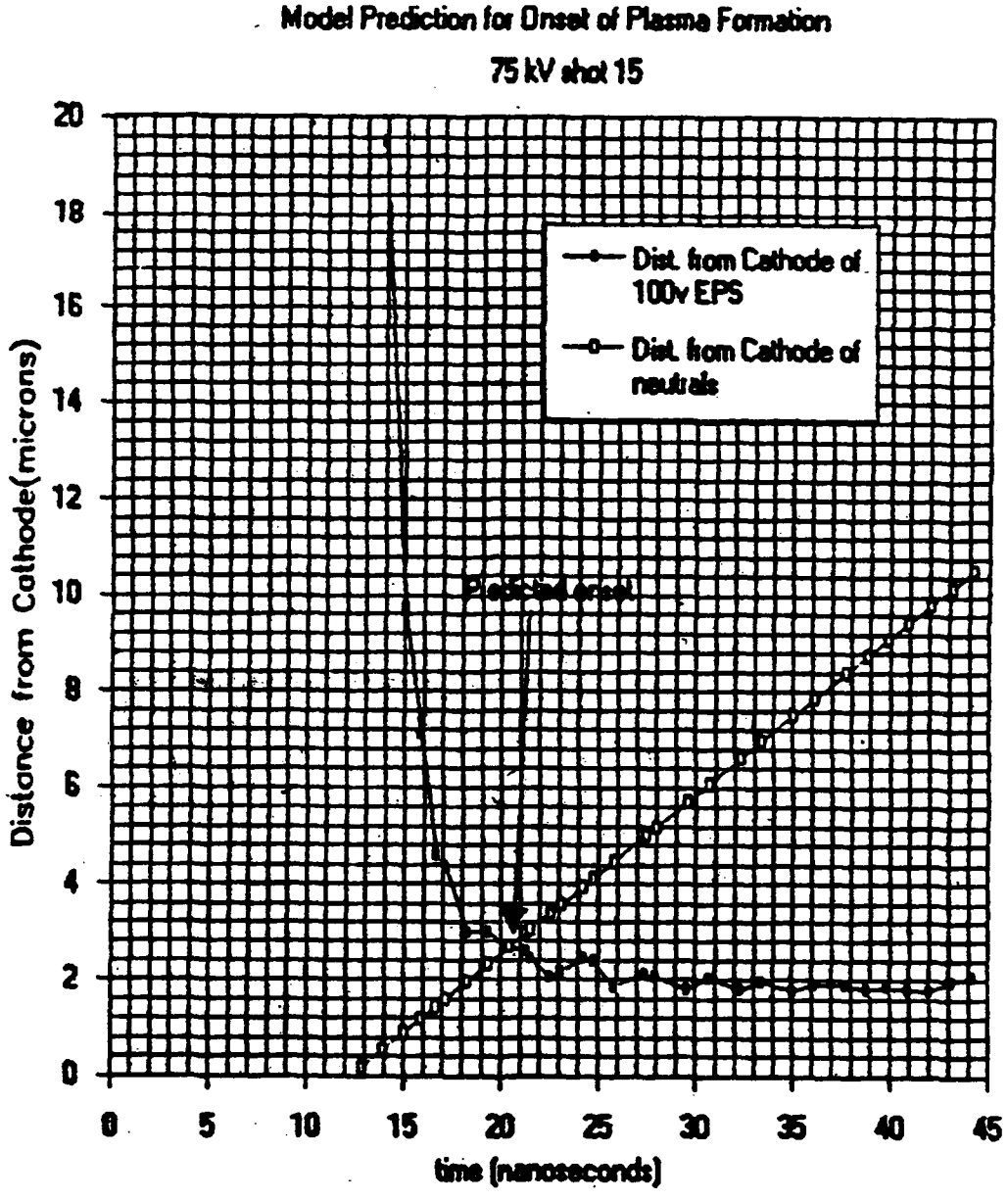

Figure 3.3 Distance from cathode of expanding neutrals and 100 V potential surface with respect to time. Predicted delay from voltage onset ≈ 8 ns [Ref. 2].

Secondary electrons produced by ionization a few micrometers from the anode have a much higher ionization cross section. Their mean free path length is approximately 1 μm. They

will ionize the desorbed dense neutral gas layer very efficiently.

Therefore is reasonable to assume that sufficient ionization at the anode will be achieved in a time frame on the order of neutral desorption and expansion at the cathode, a few nanoseconds [Ref. 6]. The time of flight of the electrons is negligibly small.

Having made those assumptions, it is a safe prediction that the delay in onset of plasma formation in the anode and cathode regions of the diode should be roughly the same. The initial ionization will start with the onset of the electron current through the gap. Initially, as the voltage pulse builds, the displacement current will dominate the current until the increasing electric field leads to field emission of electrons. Once breakdown and plasma formation on the cathode occurs, the electron current will provide ionization of neutrals on or near the anode surface.

IV. EXPERIMENT

A. OVERVIEW

The purpose of this experiment is to determine whether plasma formation occurs at the anode, and if so, determine the time delay in onset of plasma formation relative to the voltage pulse. Additionally, these same parameters will be determined for plasma formation at the cathode, so that a comparison can be made to the model discussed in Chapter III.

The diode used in this experiment is the fast-pulsed vacuum diode at the Naval Postgraduate School Flash X-Ray (FXR) facility. The FXR machine is capable of delivering a 1.7 MV, 20 ns (FWHM) pulse across the diode. System specifications of the FXR machine are listed in Table 4.1 [Ref. 9]. The basic layout of the facility is shown in Figure 4.1. Diode voltage and current are measured by permanently installed monitors. The primary source of light emitted from the diode is due to de-excitation and recombination within the plasma [Ref. 10]. This light emission is observed through a viewing window installed on the diode chamber, and focused onto a Si type avalanche photodetector. The voltage and photodetector signals are monitored on two 1 GHz bandwidth Tektronix 7104

oscilloscopes and processed using the Tektronix Digital Camera System (DCS). The diode current is monitored on a 1 MHz bandwidth Tektronix 7904 oscilloscope and photographed. Additional information on the monitoring package is provided in Appendix A.

Table 4.1 NPS FXR CHARACTERISTICS

Marx Generator:	
Stages	12
Stage Capacitance	.0.05μf
Max. Charge Voltage	1.0 kV
Max. Energy Stored	3 kJ
Blumlein Generator	
Output Impedance	43 ohms
Output Voltage	1.7 MV
Pulse Width (FWHM)	20 ns

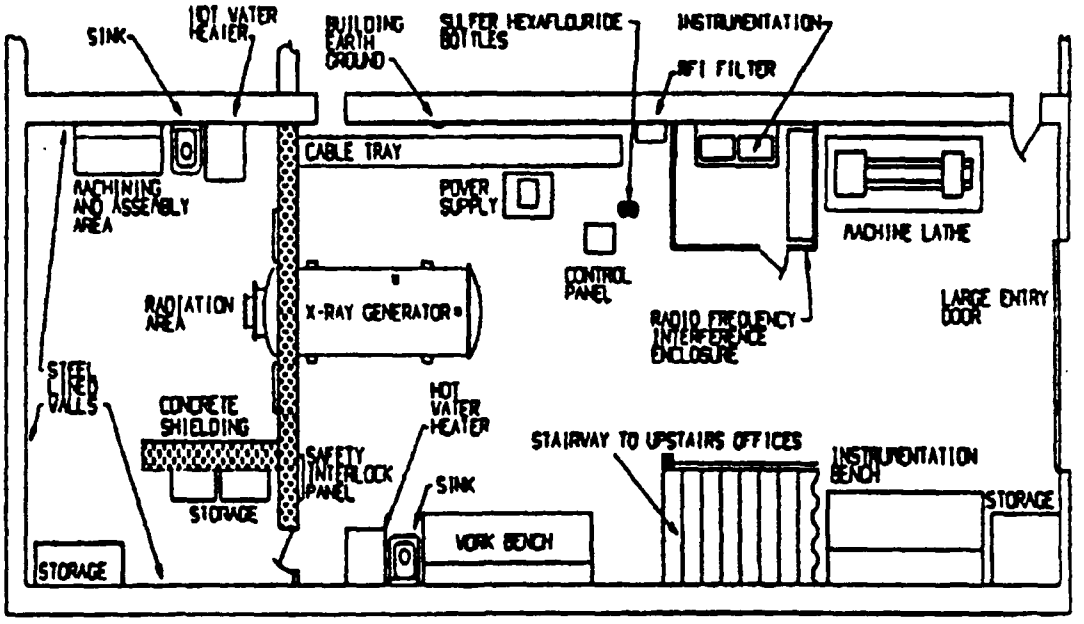

Figure 4.1 Basic floor plan of NPS Flash X-Ray facility.

B. EXPERIMENTAL CONCERNS

1. Timing

The parameters in question for this experiment are in nanosecond time frames. The diode voltage, diode current and photodetector signals must be precisely resolved in time. These pulses have rise times of less than 10 ns, making put-through times, triggering deviations, etc., very important. All of which must be accounted. Synchronization procedures, to include accounting for optical delays as well put-through times, are described in Appendix B.

2. EM noise and X-Ray Emission

• The operation of the FXR generates a wide spectrum of electromagnetic noise and X-Rays. Previous experience or "corporate knowledge" greatly reduced problems encountered in this area. The following precaution were taken:

• The oscilloscopes, delay generator and DCS were located in the radio interference (RFI) enclosure at the pulse forming end of the FXR machine;

• all cabling and connectors near either end of the machine were shielded with aluminum foil;

• an additional RFI enclosure was constructed around the photodetector and power supply; and

• dark signals (no light permitted at photodetector) were taken and subtracted from actual signals to reduce the effect of noise on the very small (<20 mV) photodetector output.

These precautions greatly reduced the noise and provided clear signals for later analysis.

C. EXPERIMENTAL SETUP

The following is an overview of the location and purpose of the optical and electronic components comprising the data acquisition package. Further details regarding

operation and specifications of these components is presented in Appendix A.

1. Optical Setup

As shown in Figure 4.2, a three lens focusing system, focused at a point at a point on either the cathode or anode surface, was used to gather and direct the plasma emitted light into a 3 m x 5 mm fiber optic cable. The fiber optic cable focused the light onto a Opto-Electronics, Inc. PD-30 series photodetector. The detector, equipped with its own biasing power supply, was biased to -125 V.

2. Electronic Setup

The diode voltage and photodetector signals were directed to two Tektronix 7104 oscilloscopes. The current signal was monitored using a Tektronix 7904 oscilloscope. In order to synchronize the signals, a common reference (t_o) trigger was required. This reference was provided by the Marx voltage signal, which precedes the diode voltage

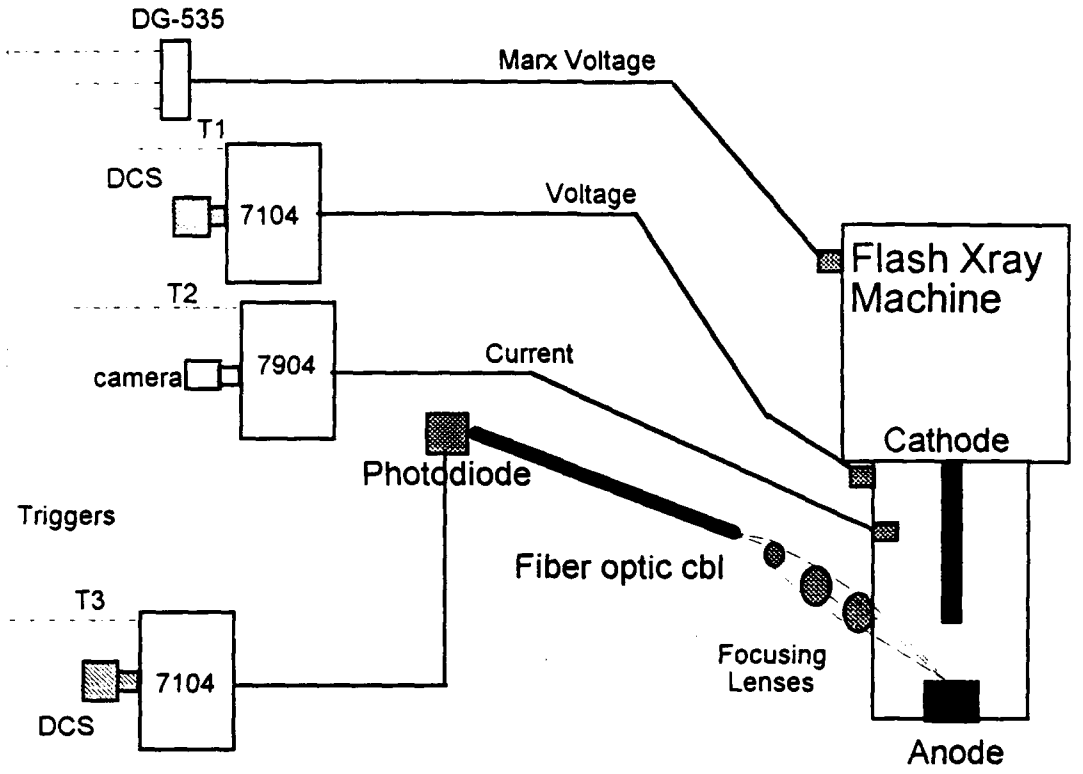

Figure 4.2 Schematic diagram of experimental setup. Position shown is for observation of Anode.

by some 300 ns. This delay also facilitated the triggering, put-through and acquisition of the waveform with the Digital Camera System (DCS), as well as utilization of the Stanford Research DG-535 multi-channel digital delay generator. The total delay through the data acquisition system was approximately 140 ns. The Marx signal was input into the DG-535 delay generator and delays programmed into each channel prior to each run. Each DCS set for external trigger which is provided by the gate out signal from its respective oscilloscope. The process was then:

a) Marx trigger to DG-535;

b) DG-535 starts counting and when a programmed delay time is reached it sends a trigger pulse to that oscilloscope;
c) Oscilloscope triggers and sends trigger pulse to the DCS;
d) DCS shutter opens to capture oscilloscope presentation.

A timing reference run was performed prior to each run in order to resolve delays between the signal paths. This was done by providing a simultaneous reference signal at both the diode voltage and photodetector input, and then, using DCS, the difference in arrival times on each system was measured. The average of ten consecutive pulses was then used as the timing differential for the cable paths. Optical delays and rise-times were also accounted for and a standard delay for the non-cabled transmission path was calculated and is figured into each programmed delay. A more complete presentation of timing synchronization procedures is in Appendix B.

D. PROCEDURE

1. Setup

A. Optics

Align optics. Turn on photodetector power supply and adjust bias to -125 V. Test detector by placing a light source in optical path and observing a deflection in the power supply voltage meter. Inspect diode chamber and window for abnormalities, e.g. cracks.

b. FXR

Turn on ion gauge and verify sufficient vacuum, normally around 2.5 x 10^{-5} torr. Set pressure switches per FXR maintenance and operation manual.

c. Setup Data Acquisition Package

Turn on instruments and allow 30 minutes warm-up. Verify wiring. Adjust oscilloscope settings, DG-535 input/output settings, etc. Calibrate and scale DCS.

2. Timing checks

The timing procedure outlined in Appendix B must be performed prior to each data run, and after any change is made in instrument settings. Calculate time differential and add/subtract 18.6 ns for optical path delay (discussed in Appendix B) as necessary. Program DG-535. Test triggers by placing DG-535 in 'single-shot' mode, setting DCS to acquire (w/ext. trigger). Scope single sweep ready lights should illuminate; DCS should indicate standby mode. Then manually trigger the delay generator.

3. Observations

Record all observations to include diode vacuum, gap separation, Marx charge, qualitative condition of electrodes, etc.

4. Data run

(1) Set DCS external trigger. Press F1 for acquisition. Oscilloscope single sweep ready lights will illuminate.

(2) Open shutters on diode current oscilloscope camera, if applicable.

(3) Insert keys, and Charge Marx bank to desired voltage.

(4) When charging is complete (Charge complete and FIRE Lights will illuminate), FIRE the FXR.

(5) Return both keys to safe position. Secure high voltage source.

(6) Close camera shutters and remove exposed film.

(7) Repeat steps 3-6 as necessary.

(8) To obtain a noise reference or "dark" signal, cover photodetector aperture and repeat steps 3-6.

V. RESULTS

A. TIME RESOLVED PLASMA FORMATION

1. Measurement Error

An analysis of measurement errors has been performed and is contained in Appendix C. This analysis indicated an error in voltage measurements of ±10% and a ±15% error in current measurements. The timing measurement error is ±1 ns.

2. Data

In general, 10 shots were fired per data run. Six data runs were performed at a Marx charge voltage of 75 kV, which corresponds theoretically to 1.04 MV across the diode. The experimental average peak diode voltage was 0.96 MV, which differs from the standard by 7.6%, and is within the voltage measurement error. Figures 5.2-5.5 show the DCS presentation of a diode voltage signals. For comparison Figure 5.1 is an earlier photograph of the oscilloscope trace of a typical diode voltage signal.

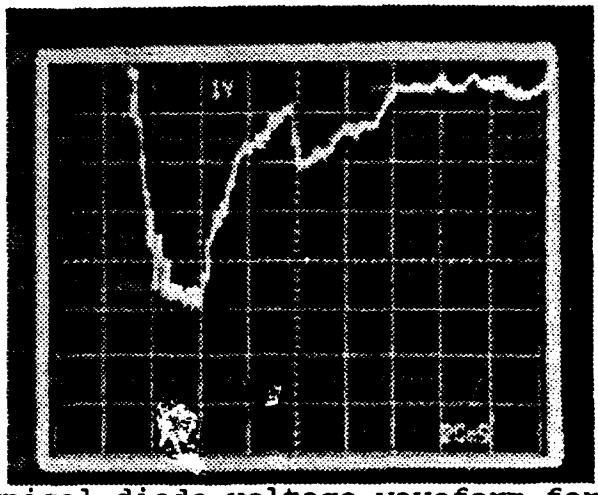

Figure 5.1 Typical diode voltage waveform for 75 kV Marx charge shot. (46 dB attenuation at oscilloscope input)

Figure 5.2 is shows the DCS presentation of an anode light intensity signal and diode voltage signal acquired in this experiment. Note the delay in onset of the light emission from that of the diode voltage. The average value of this delay of onset of plasma formation at the anode was 6.5 ±1 ns, with a standard deviation of 1.7 ns. Figure 5.3 shows the DCS presentation of an cathode light intensity signal and diode voltage signal. Again, note the delay in onset of plasma formation at the cathode. The average value of this delay was 7.9 ±1 ns, with a standard deviation of 0.9 ns.

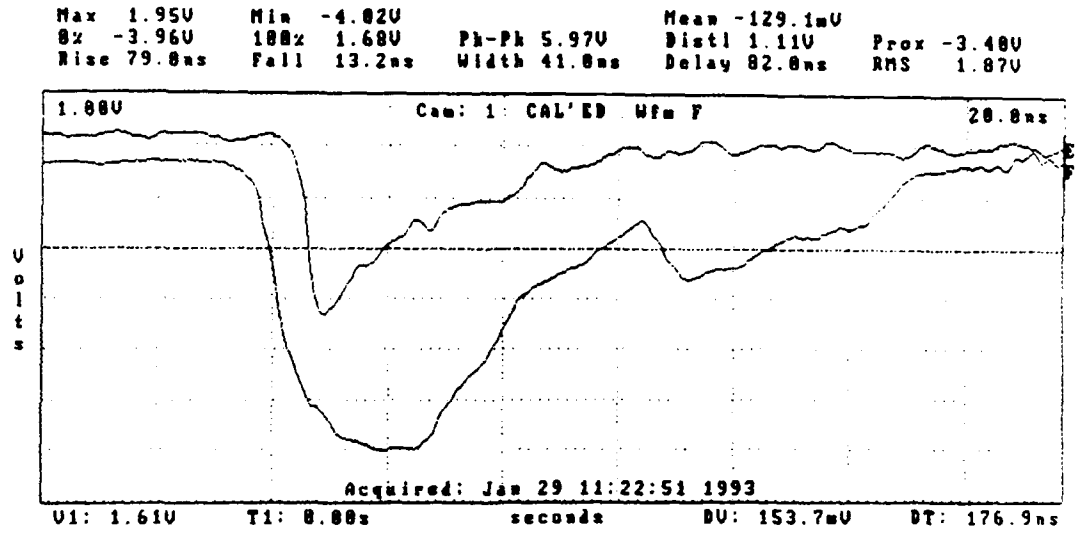

Figure 5.2 Anode Plasma Emission (top) and Diode Voltage signals for 75 kV Marx charge shot. Note the delay between onset of signals.

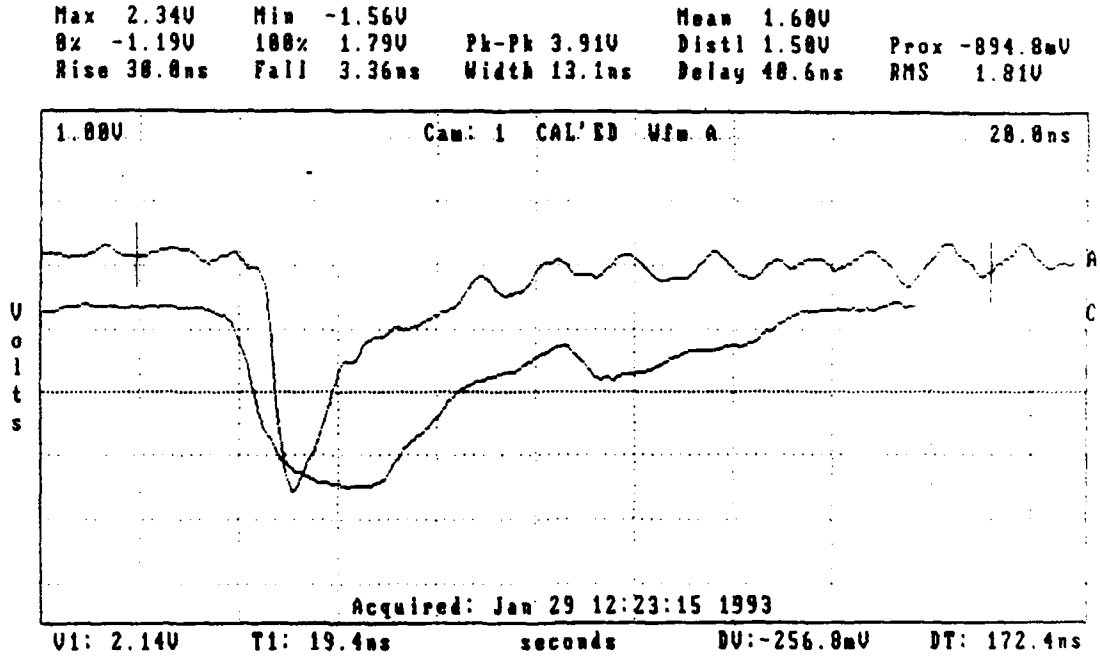

Figure 5.3 Cathode Plasma Emission (top) and Diode Voltage signals for 75 kV Marx charge shot. Note the delay between onset of signals.

Figure 5.4 is a presentation of the averaged anode plasma emission, cathode plasma emission and diode voltage signals for a one 10 shot run. The plasma emission signals are averaged over five consecutive shots each, and the diode voltage averaged over the entire data run. Figure 5.5 and 5.6 graphically illustrates the variations in diode voltage in the data.

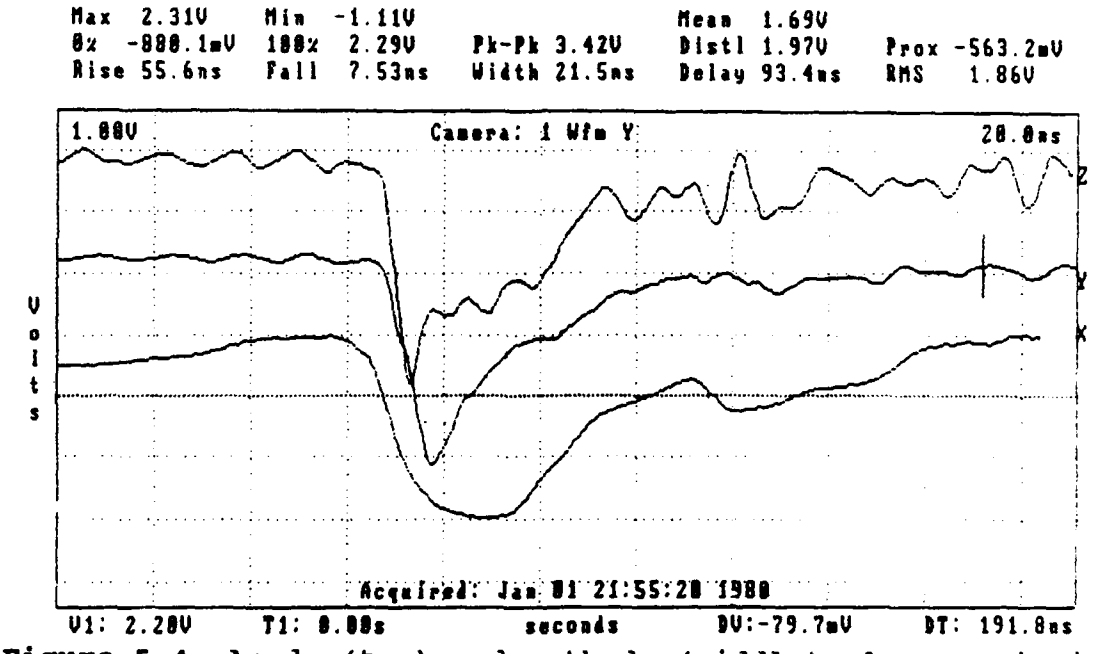

Figure 5.4 Anode (top) and cathode (middle) plasma emission and diode (bottom) voltage signals averaged over 5 shot data run. Plasma emission signals are vertically scaled. All signals are synchronized.

Again, the delay in onset of plasma formation is evident. This figure also shows plasma formation at both electrodes occurring at roughly the same time. This is supported by the complete data set in the average onset delays reported above.

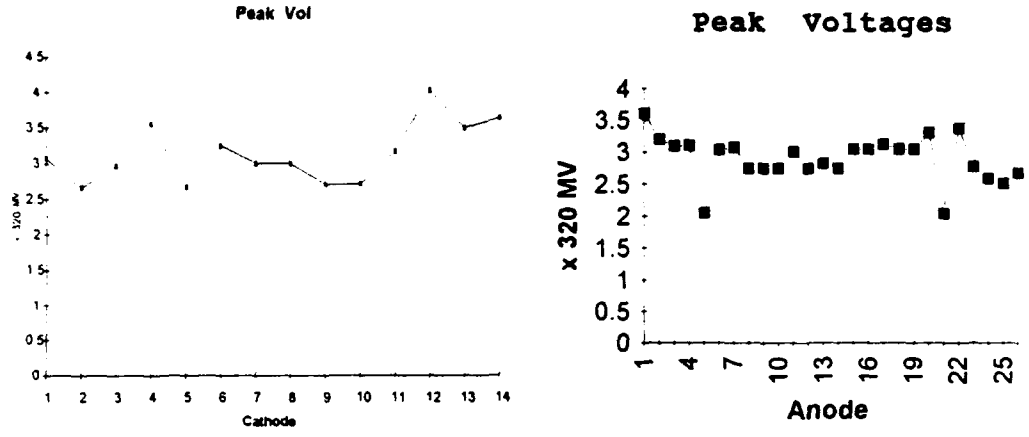

Figures 5.5 and 5.6 Plots of the diode voltage for cathode (left) and anode shots in the data series. These plots show the degree of variation in the data.

In Figures 5.7 and 5.8, the onset of diode voltage is plotted with the onset of plasma formation at the anode and cathode, respectively. Note that in general, the two parameters vary in the same fashion--an earlier onset of voltage corresponds to an earlier onset of plasma formation. Also, the delay of onset of plasma formation is represented by the tie-line.

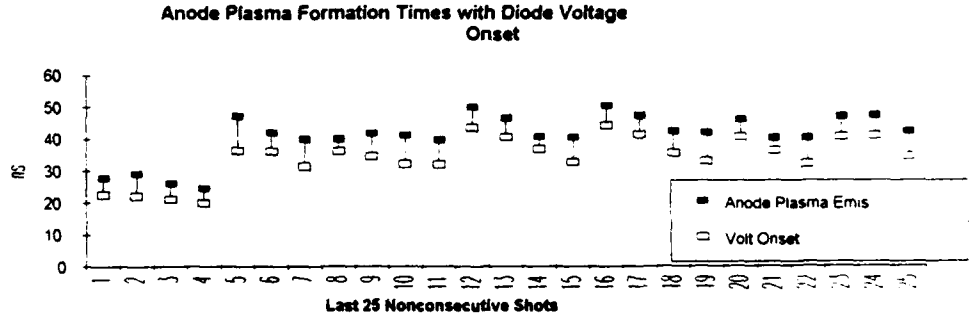

Figures 5.7 Plot of onset times for diode voltage and plasma emission for last 25 observations of anode.

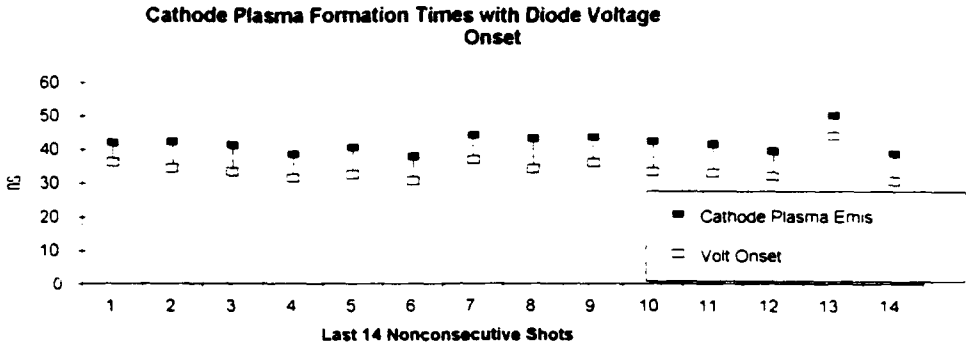

Figures 5.7 Plot of onset times for diode voltage and plasma emission for last 25 observations of cathode.

Several other parameters were of interest, including the risetimes of the respective plasma emissions, emission intensities, voltages at onset, and others. These parameters are listed in Table 5.1. All times are relative to the Marx pulse, t_o. The parameters listed are:

1) Plasma emission (t2) - onset of intensity signal;
2) Plasma FWHM - time to half max of signal;
3) Plasma Pk - time to signal peak;
4) Pk Int - Peak photodetector output;
5) Volt onset - time to voltage onset;
6) Pk volt - peak voltage
7) Volt @ t2 - voltage at onset of intensity signal;
8) Volt @ t3 - voltage at half max of intensity;
9) Delay1 - voltage onset minus intensity onset;
10) Delay2 - voltage onset minus half max intensity;
11) Delay3 - voltage onset minus peak intensity; and
12) Risetime - risetime of intensity signal.

TABLE 5.1 FINAL STATISTICS FOR ANODE AND CATHODE DATA SETS

	Plasma Emis	Plasma FWHM	Plasma Pk	Pk Int	PW	Volt Onset	Pk Volt	Volt @ t2	Volt @ t3	Delay1	Delay2	Delay3	Risetime
	t2	t3	t4	I(pk)	PW	t1	V(pk)	V(t2)	V(t3)	t2-t1	t3-t1	t4-t1	
	ns	ns	ns	**7.31**	ns	ns	**x 320**	**x 320**	**x 320**	ns	ns	ns	ns
ANODE:													
AVG VALUE	41.6	49.2	54.2	29.8	38.9	34.9	2.9	1.2	2.0	6.5	15.0	20.5	2.8
MAX VALUE	59.7	69.0	100.0	47.7	51.3	50.5	3.6	1.7	2.7	10.8	33.1	63.7	5.6
MIN VALUE	24.4	43.1	21.7	19.2	6.7	19.8	2.0	0.7	1.3	3.8	8.4	11.5	1.8
STD DEV	7.8	5.4	13.8	10.3	10.6	7.4	0.4	0.3	0.4	1.7	8.7	15.7	1.1
CATHODE:													
AVG VALUE	41.8	46.3	49.7	40.0	30.2	34.1	3.1	1.5	2.4	7.9	12.1	15.7	3.4
MAX VALUE	50.3	53.4	55.8	58.9	43.4	44.0	4.0	2.2	3.0	9.6	17.2	22.8	5.7
MIN VALUE	37.7	43.3	46.6	21.5	7.6	30.5	2.7	0.9	1.9	6.3	10.2	12.3	2.4
STD DEV	3.2	2.9	2.9	12.5	13.0	3.5	0.4	0.3	0.4	0.9	1.8	2.4	0.9

One additional interesting item in Table 5.1 is the slight difference in risetimes (about one-haft nanosecond) between anode and cathode plasma emissions. The slightly more quickly rising anode plasma emission pulses are also evident in Figures 5.2-5.4. This small difference is within the 1 ns error determined in Appendix B, and may be insignificant.

B. PHOTOGRAPHY

Following numerical data acquisition, the anode surface was observed through optical microscopy. Figures 5.9 and 5.11 show the presence of sparse craters on the anode surface. For comparison Figure 5.10 is an earlier photograph of cathode spots.

Figure 5.9 Photographs of Anode surface following a 5 shot series showing the formation of craters on the anode surface. (200X)

Figure 5.10 Photograph of Cathode surface showing formation of craters, or cathode spots, on the surface. Courtesy of F. Schwirzke.

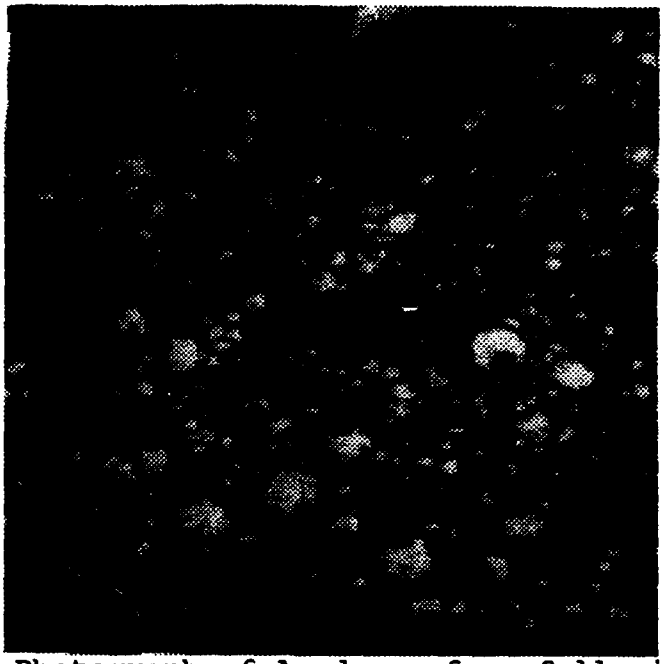

Figure 5.11 Photograph of Anode surface following a five shot series showing formation of craters on the anode surface. (500X)

C. COMPARISON TO MODEL

Firstly, the model predicts that a plasma will form at the anode surface. The anode plasma intensity measurements support that prediction.

Secondly, in the case of plasma formation at the cathode, the experimental value of 7.9 ±1 ns for the delay in onset compares excellently to the model prediction of 8 ns. In Chapter III it was estimated that the onset of plasma formation on the anode should roughly equal that on the cathode, about 8 ns. The experimental value was 6.5 ±1 ns.

Lastly, it was also proposed that plasma-surface interaction, specifically, unipolar arcing, occurs at both the cathode and anode plasma interfaces. The appearance of the small, spherical craters on the anode surface support that hypothesis.

VI. CONCLUSIONS AND RECOMMENDATIONS

A. CONCLUSIONS

The purpose of this work was to determine whether plasma formation occurs near the anode surface of a diode during a fast-pulsed high voltage event. And, if plasma formation does occur, to determine the time of onset relative to voltage onset. The results of the experiments indicate that a plasma does indeed form in the anode region. The results show that plasma formation near the anode occurs in a time frame comparable to plasma formation near the cathode. Post-event photographs of the anode surface showed the presence of craters similar to those previously found on the cathode surface. This supports the theory that uni-polar arcing occurs at the anode as well as the cathode, and that post breakdown events are occur in parallel in the two regions. It can be concluded that cathodic processes, although responsible for the field emission of electrons, do not necessarily dominate these events in terms of the plasma production and expansion which leads to gap closure.

B. RECOMMENDATIONS

While the methods used to time resolve the signals in this work are reasonable, direct comparison of the plasma

formation onset times for the respective electrodes would best be done by simultaneously observing the cathode and anode surfaces.

Additionally, desorption on the electrode surfaces, a key aspect in plasma formation, is greatly dependent on the particular molecules adsorbed to the surfaces. Determination of these molecules is necessary for an exact quantification of the desorption process.

APPENDIX A: DATA ACQUISITION PACKAGE

A. DIODE VOLTAGE SENSOR

The NPS FXR diode voltage is measure with the PIM-197A-25 voltage divider. The primary divider is a 40 cm long flexible tube filled with electrolyte. The sensor is designed to match a 50 ohm oscilloscope input impedance. Several important specifications are listed in Table A.1.

B. DIODE CURRENT SENSOR

The diode current is measure by the PIM-199B flux meter. The flux meter is single turn, inductively coupled flux probe. Its output is proportional to the flux linking the turn [Ref. 11]. Several important specifications of the diode current sensor are listed in Table A.2.

Table A.1 DIODE VOLTAGE SENSOR (PIM-197A-25) CHARACTERISTICS

Peak design voltage (MV)	2.0
Max. pulse length (ns)	200
Rise time (ns)	1.5
Accuracy (%)	±5
Sensitivity (kV/V)	1.6

Table A.2 DIODE CURRENT SENSOR (PIM-199) CHARACTERISTICS

Rise time (ns)	0.4
Sensitivity (V/T)	875
Accuracy (%)	±5
Loop diameter (cm)	2.5

C. PHOTODETECTOR

The photodetector used to measure the plasma's light emission was the Opto-Electronics, Inc., Series PD-30 Ultra High-Speed Photodetector. It employs an avalanche-type Si photodiode and is designed to detect and accurately resolve weak, ultra short visible light pulses. The detector is equipped with its own power supply to provide the bias voltage. The detector has a rise time of 50 ps. Figure A.1 shows the detectors response to a 100 ps pulse.

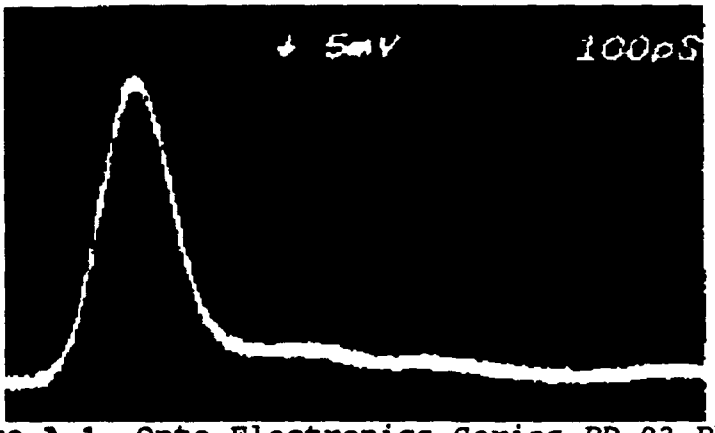

Figure A.1 Opto-Electronics Series PD-03 Photodetector response to 100 ps input pulse.

D. DIGITIZING CAMERA SYSTEM

1. Overview

The Digitizing Camera System (DCS) consists of a charge-coupled-device (CCD) camera, an IBM-PC-compatible video Frame Store Board, and associated software. It digitizes analog waveforms displayed on oscilloscope CRT screen. The capture of transients with pulse widths on the order of 500 ps is possible when used in conjunction with a fast oscilloscope, like the Tektronix 7104 used in this experiment. This system provides an accurate and efficient method to digitally record, analyze and store oscilloscope waveforms.

2. System requirements

The required equipment for operation of the DCS is:

- IBM-PC-compatible computer with 384k bytes minimum available memory.
- PC-DOS version 2.1 or higher.
- Graphics monitor with Hercules adapter, color graphics (CGA) adapter, enhanced graphics (EGA) adapter, or VGA adapter (in EGA mode).

3. Special setup considerations

Setup procedure for DCS are presented clearly in Reference 13, and standard connections are shown in Figure A.2. Figure A.3 shows the CCD camera and its connections. However, due to the ultra-short pulses observed in this experiment, it Is recommended that the scaling and

calibration procedures be performed using an outside source pulse of width (FWHM) comparable to the width of the pulse being observed. In this experiment, a 20 MHz calibrated pulse was used to scale and calibrate the DCS. This provided an error on the order of 500 ps in the DCS output, which is acceptable with respect to the data in question.

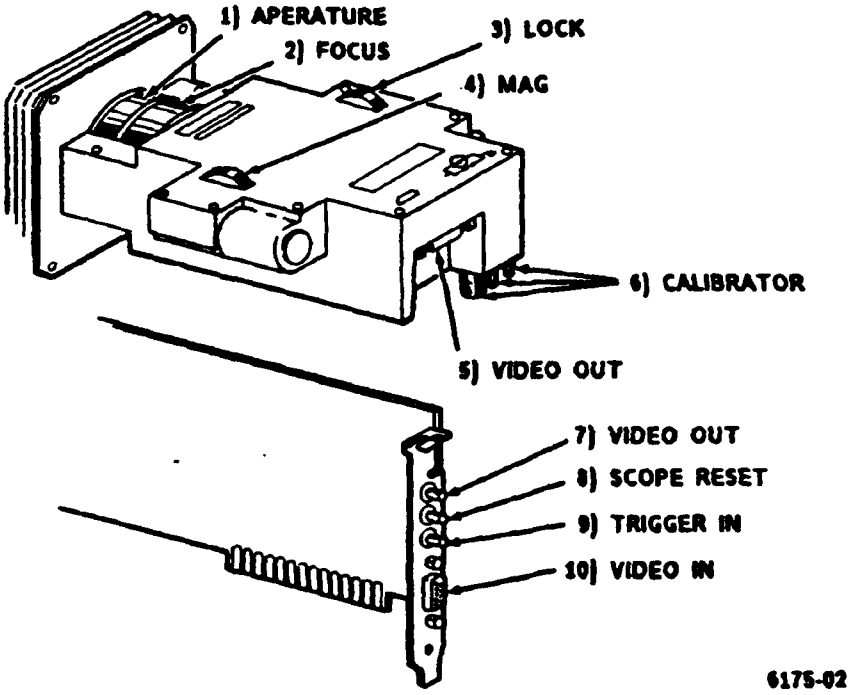

Figure A.2 DCS CCD camera showing input and output connections [Ref. 12]

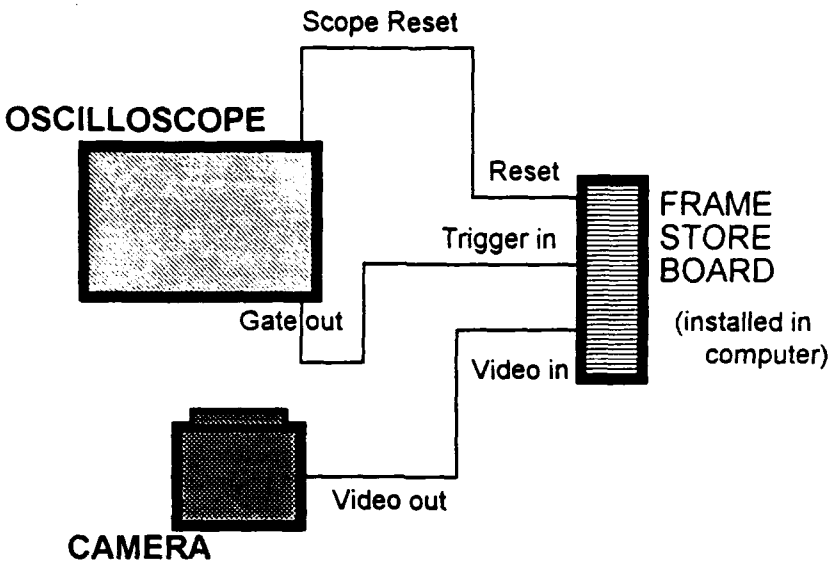

Figure A.3 Schematic of Digitizing Camera System connections [Ref. 12].

E. WAVEFORM ANALYSIS/INTERPRETATION

1. Voltage waveforms

The diode voltages measure in this experiment used 46 dB attenuation at the oscilloscope input. This attenuation, along with the sensitivity of the oscilloscope must be accounted for in converting the oscilloscope trace into actual voltages. The relation used to make this conversion is

$$V = \frac{V_o}{attenuation} \times sensitivity = V_o \times 200 \times 1.6, \qquad (A.1)$$

where

V_O≡voltage (V) read from oscilloscope; and

V≡actual voltage (kV) [Ref. 13].

2. Current waveforms

The diode current measurements of this work use 20 dB attenuation. The formula for conversion of oscilloscope trace currents to actual currents is

$$I = \frac{V_o}{attenuation} \times \frac{2\pi R}{\mu_o \times sensitivity} = 7.31 \times V_o \qquad (A.2)$$

where

V_O≡voltage (V) read from oscilloscope; and

R≡distance between diode and flux meter centers;

m_O≡permeability of free space $4\pi x10^{-7}$; and

I≡actual current (A) [Ref. 11].

APPENDIX B: TIME RESOLUTION

A. SYNCHRONIZATION OF VOLTAGE AND PHOTODETECTOR SIGNALS

1. Discussion

Due to the differences in the time base settings, jitter, and triggering of the oscilloscopes and delay generator, along with differences in transmission paths, it is essential that the output waveforms be synchronized prior to acquisition. Post acquisition time resolution of the signals to be compared is possible, but the time differential resulting from the numerous aforementioned delays would have to be calculated, being careful to account for the error in each.

In order to diminish the errors associated with post-acquisition time resolution, the time differential for the entire system (sensor input to DCS output) was measured, using a considerable sample size (10 measurements). The average of these measurements was taken as the time differential between the system acquiring the voltage signal and the system acquiring the photodetector signal. This procedure is reasonable since the data in question is of a relative nature, i.e., the difference in onset of each pulse.

This time differential was then added to the standard optical path delay for the photodetector signal,

which is presented later in this chapter, and programmed as a delay in the appropriate trigger, thereby resulting in a synchronized DCS output.

2. Method

1. Disconnect diode voltage sensor and photodetector output cables. Connect both to a tee connector.

2. Setup and connect 20 MHz pulse generator (PG) to input of tee connector. Set generator output for a repetitive 20 ns pulse, with a 100 ns advance trigger. Connect advance trigger to extra cable entwined with photodetector signal cable (labeled A or B depending on which is used for p/d signal).

3. Connect advance trigger to external trigger input of DG-535 delay generator (DG). Verify DG output settings, i.e., slope, impedance, etc. are correct. Connect DG outputs to appropriate oscilloscope. Set delays to zero.

4. Adjust oscillcscope trigger in order to view waveform. Adjust settings to those to be used for data acquisition and use attenuators as necessary for presentation of the complete waveform.

5. Set PG to manual. Set oscilloscope triggers to external. Set DCS to acquire.

6. Trigger the pulse generator.

7. Pulses should be presented on each computer terminal. Record time of pulse onset for each system. Calculate time differential.

8. Repeat 4 and 6 as necessary. Generally, 10 measurements were taken. The concern is obtaining a sample with a standard deviation <500 ps--about the error in reading the DCS output.

It was noted that the average time differential varied by a few nanoseconds from day to day. It was therefore necessary to conduct a timing run prior to each data run. Use of the DCS and an HP-48SX statistics program made this task relatively simple.

B. DETERMINATION OF OPTICAL DELAY

1. Discussion

The light emitted from the plasma must travel 76 cm through the diode chamber and lensing system, then through 3 m of fiber optic (F/O) cable. The cable path time differential described above does not account for this additional delay in the photodetector signal.

This would be a simple calculation provided the index of refraction of the fiber optic cable were given. However, this was not the case, and the optical delay through the F/O cable had to be determined experimentally.

2. Method

The setup used to determine the f/o cable optical delay is shown in Figure B.1. A Xenon Corporation model 437A Nanopulser was used as the light sources. Its output was a 20 ns light pulse. The nanolamp was place 0.5 m from the f/o bundle. The photodetector was connected to a Tektronix 7104 oscilloscope and DCS. The DCS was set to light trigger. The nanolamp was manually triggered and the output acquired by DCS. The time of arrival of the light pulse was recorded.

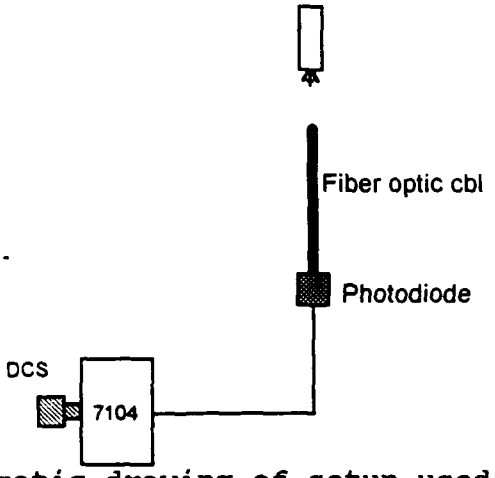

Figure B.1 Schematic drawing of setup used to determine optical delay of fiber optic cable. The f/o cable is removed to acquire the reference signal.

The f/o cable was then removed and, leaving all other components in place. The nanolamp was again triggered. The waveform was captured and time of arrival recorded. This process was repeated 36 times, at which point standard deviation of .95 ns was achieved. The average optical delay of the fiber optic bundle was 15 ± 1 ns.

The delay in transmission of the light pulse from the electrode surface corresponds to 2.5 ns. The total optical path delay was 18 ±1 ns.

APPENDIX C - ERROR ANALYSIS

A. VOLTAGE AND CURRENT MEASUREMENTS

This section describes the error in all measurements involving voltages read from signals, i.e., vertical deflection of the oscilloscope. Applicable component accuracies are provided in table C.1.

Table C.1 VOLTAGE AND CURRENT MEASUREMENT ACCURACIES

Voltage sensor	±5%
Current sensor	±5%
Attenuation*	±5%
Oscilloscope plug-in units (7A29)	±2%
Visual interpretation - Current*	±10%
Visual interpretation - Voltage**	±5%
Digitizing Camera System	±0.3%

*Historical estimate.
**Estimate based on utilization of DCS software.
All other values based on manufacturer's specifications

These are independent errors and can therefore be added in quadrature [Ref. 14]. The total error in voltage measurements is ± 10%. The total error in current measurements (DCS not used) is ±15%.

B. TIMING MEASUREMENTS

This section deals with errors involved in all timing measurements, i.e., horizontal deflections on the oscilloscope. Applicable component errors are listed in

table C.2. The time measurements of this work are relative to voltage onset. The timing differential described in Appendix B accounts for the average errors in individual components, such as time base errors, jitter, etc. These errors are not applicable to these measurements.

The only remaining error relative to the data presented in this work is that of visual interpretation of the DCS outputs, which, based on experimenter's experience and a scale factor of 1.11 ns/mm, is conservatively estimated to be ±0.6 ns. The total error in time measurements is rounded to ±1 ns.

LIST OF REFERENCES

1. Schwirzke, F., Murayama, X.K. and Minnick, S.A., **Onset of Breakdown in a Vacuum Diode**, Proceedings of the Eighth International Conference on High-Power Particle Beams, Vol. 2, World Scientific, Singapore, p. 985, 1991.

2. Hallal, M.P. Jr., **The Onset of Breakdown in a Fast Pulsed Vacuum Diode**, M.S. Thesis, Naval Postgraduate School, Monterey, California, June 1991.

3. Schwirzke, F., **Laser Induced Breakdown and High Voltage Induced Breakdown on Metal Surfaces**, Laser Interaction and Related Plasma Phenomena, H. Hora and G. H. Miley, ads., Plenum Publishing Corporation, 1991.

4. Miller, R.B., **An Introduction to the Physics of Intense Charged Particle Beams**, Plenum Press, 1982.

5. Barnett, C.F., Ray, J.A., and Thompson, J.C., **Atomic and Molecular Collision Cross Sections of Interest in Controlled Thermonuclear Research**, p. 141, Oakridge National Laboratory, August 1964.

6. Schwirzke, F. and Hallal, M.P., **Explosive Plasma Formation on Electrodes**, paper presented at the Annual Meeting-APS Division of Plasma Physics, 32nd, Cincinnati, Ohio, 12-16 1990.

7. McDaniel, E.W., **Collision Phenomena In Ionized Gases**, John Wiley & Sons, 1964.

8. Barnett, C.F., Ray, J.A., Thompson, J.C., **Atomic and Molecular Collision Cross Sections of Interest in Controlled Thermonuclear Research**, Oak Ridge National Laboratory, Oak Ridge Tennessee, 1964.

9. Pietruszka, R.B., Operation and Characteristics of the Flash X-Ray Generator at Naval Postgraduate School, M.S. Thesis, Naval Postgraduate School, Monterey, California, June 1991,.

10. Hinshelwood, D., **Explosive Emission Cathode Plasmas in Intense Relativistic Electron Beam Diodes**, Ph.D Dissertation, Massachusetts Institute of Technology, Cambridge, Maryland, January 1985

11. Physics International Company, **PIM-199 Flux meter Data Sheet,** March 1978.

12. Tektronix Company, **Digitizing Camera System**, August 1988.

13. Physics International Company, **PIM-197 Voltage Dividers Data Sheet**, March 1978.

14. Taylor, J.R., **An Introduction to Error Analysis**, Oxford University Press, 1982.

INITIAL DISTRIBUTION LIST

1. Library, Code 52 — 2
   Naval Postgraduate School
   Monterey, Ca 93943-5002

2. Professor Fred Schwirzke, Code Ph/Sw — 3
   Department of Physics
   Naval Postgraduate School
   Monterey, Ca 93943-5000

3. Professor Xavier K. Maruyama, Code Ph/Ma — 2
   Department of Physics
   Naval Postgraduate School
   Monterey, Ca 93943-5000

4. Professor Karlheinz E. Woehler, Code Ph/Wh — 1
   Department of Physics
   Naval Postgraduate School
   Monterey, Ca 93943-5000

5. Physics Library, Code PH — 1
   Department of Physics
   Naval Postgraduate School
   Monterey, Ca 93943-5000

7. LT Greg Willis — 2
   223 Willis St.
   Hattiesburg, MS 39401

8. Defense Technical Information Center — 2
   Cameron Station
   Alexandria, VA 22304-6145